A hybrid methodology for structural damage detection uniting FEM and 1D-CNNs: Demonstration on typical high-pile wharf

Demonstration on typical high-pile wharf

Zhou, Yujue; Zheng, Yonglai; Liu, Yongcheng; Pan, Tanbo; Zhou, Yubao

DOI
10.1016/j.ymssp.2021.108738

Publication date
2022

Document Version
Final published version

Published in
Mechanical Systems and Signal Processing

Citation (APA)
Zhou, Y., Zheng, Y., Liu, Y., Pan, T., & Zhou, Y. (2022). A hybrid methodology for structural damage detection uniting FEM and 1D-CNNs: Demonstration on typical high-pile wharf: Demonstration on typical high-pile wharf. *Mechanical Systems and Signal Processing*, *168*, Article 108738. https://doi.org/10.1016/j.ymssp.2021.108738

Mechanical Systems and Signal Processing 168 (2022) 108738

Contents lists available at ScienceDirect

Mechanical Systems and Signal Processing

journal homepage: www.elsevier.com/locate/ymssp

A hybrid methodology for structural damage detection uniting FEM and 1D-CNNs: Demonstration on typical high-pile wharf

Yujue Zhou [a,b], Yonglai Zheng [b], Yongcheng Liu [b,*], Tanbo Pan [b], Yubao Zhou [c]

[a] Department of Civil Engineering, Sanming University, Sanming 365004, PR China
[b] Department of Hydraulic Engineering, Civil Engineering College, Tongji University, Shanghai 200092, PR China
[c] Faculty of Civil Engineering and Geosciences, Delft University of Technology, Delft 2600AA, Netherlands

ARTICLE INFO

Communicated by Wei-Xin Ren

Keywords:
High-pile wharf
Pile foundations
Vibration
Structural health monitoring
Structural damage detection
Finite element modeling
1D Convolutional neural networks

ABSTRACT

Vibration-based structural damage detection (SDD) has been a subject of intense research in structural health monitoring (SHM) for large civil engineering structures over the decades. The performance of the conventional SDD approaches predominantly relies on the rational choices of the damage feature and classifier. Hand-crafted features or fixed classifiers would not be the optimal choice for all structural damaged scenarios. This paper proposes a novel, quick and precise real-time SDD framework for high-pile wharf foundations using a combination of finite element modeling and 1D convolutional neural networks (CNNs). The distinct advantage of this method lies in extracting the damage-related features from the raw displacement response directly and automatically, and the computational complexity of the compact 1D CNNs is significantly lower because the data processing involves only simple 1D operations. The results show that the presented 1D CNNs have a superior ability to accurately identify the occurrence and location of damage in real time. In addition, the comprehensive performance of the CNNs trained by the displacement response dataset in component form is significantly better than that based on the dataset in absolute value form. The results also demonstrated that although the proposed CNNs are more sensitive to the longitudinal and lateral displacement responses of the high-pile wharf structure, the vertical component still has a positive effect on the improvement of the generalization and robustness of the CNNs.

1. Introduction

High-pile wharfs have always been prone to the damage induced by slope deformation, ground settlement, and ship collision during their service lives. However, coastal structures need to be monitored in real time to improve their operational performance, prolong their expected life spans, reduce maintenance costs, and prevent sudden catastrophic failures [1,2]. Conventional structural damage detection (SDD) methods are laborious and costly especially due to the lack of highly trained labor and safe access to the surface of the monitored structural components [3]. Therefore, efficiently detecting and precisely locating the structural damage in foundations of high-pile wharfs have always been formidable challenges for the research community.

Past decades have seen the rapid development of reliable vibration-based structural damage detection (VSDD) techniques which have been adopted by most structural health monitoring (SHM) systems and become the standard method in practice at this stage. For

* Corresponding author.
E-mail address: 1930156@tongji.edu.cn (Y. Liu).

https://doi.org/10.1016/j.ymssp.2021.108738
Received 14 August 2021; Received in revised form 5 December 2021; Accepted 7 December 2021
Available online 20 December 2021

instance, Ghiasi et al. [4] utilized the kernel method to identify the structural damage based on structure dynamic responses. Fan et al. [5] made a comprehensive review of the damage identification methods based on dynamic characteristics in the first ten years of the 21st century and conducted experimental research on beam members using different damage identification methods. The results showed that damage identification methods based on mode shape and frequency are difficult to locate damage. Similarly, Hou et al. [6] have made a systematic review of damage identification methods based on dynamic characteristics in the past ten years and pointed out the basic premise of such methods is that the physical properties change due to damage, which in turn affects the modal properties of the system. Farrar et al. [7] concluded that damage identification based upon changes in vibration characteristics is one of the few methods that monitor changes in the structure on a global basis. Based on the existing research results, VSDD techniques can be divided into two classes: parametric and nonparametric approaches. Parametric approaches identify structural damage by analyzing the before and after changes in damage-sensitive dynamic parameters [8]. However, nonparametric approaches realize the goal by extracting the damage-sensitive features directly from the dynamic response [9]. Despite the wide application of VSDD methods, some common drawbacks remain. Concerning parametric approaches, global dynamic parameters are less sensitive to local damage which mainly affects the parameters in the lower-order modes [10]. Instead, the higher-order modes are very difficult to excite in engineering practice which means the corresponding modal parameters are difficult to extract accurately. Furthermore, the accuracy of model parameters is highly susceptible to external factors, such as the temperature, humidity, and measurement noise [11]. Conversely, nonparametric methods utilize statistical modeling to extract structural damage-related information from the filtered dynamic response. However, the implicit relationship between the structural damage response and these common statistical features makes it difficult to extract the required information effectively. Additionally, some nonparametric approaches are extremely sensitive to the outliers caused by environmental changes, namely, the robustness of such methods is poor.

In recent years, the capability of machine learning (ML) algorithms to model complex nonlinear relationships has increased significantly. The available ML-based SDD approaches involve two main tasks: feature extraction and feature classification [12]. The superior performance of such methods is highly dependent on the extraction of the damage-sensitive features as well as the training of suitable classifiers [13,14]. In general, these methods are likely to exhibit poor SDD performance due to the fixed hand-crafted features or the unreasonable classifiers. However, appropriate choices need to rely on the manual labor of experts who are expensive and scarce human resource. Besides, there is no guarantee that a particular feature/classifier set is the optimal choice for all types of structural damaged scenarios.

Convolutional neural networks (CNNs), as a type of multilayer feedforward neural network, are extensively used in various supervised classification tasks in the field of Deep Learning (DL). Standard 2D CNNs are suitable for processing 3D or 4D tensors, like images, videos, etc [15]. Currently, many exploratory studies have been conducted on engine and gearbox fault detection, electrocardiogram (ECG) signal classification, voice recognition, etc [16]. However, a large number of the samples in the field of SDD are time series, such as vibration and strain history. As an alternative, a 1D CNN is further developed on this basis. Recently, 1D CNNs have reasonably become a state-of-the-art technique to address vibration-based SDD/SHM issues in civil structures. In a novel and pioneering work developed by Abdeljaber et al., the raw multipoint dynamic response, which was measured from a large-scale steel structure frame model under specific excitation, was used to establish a 1D CNN-based structural damage identification model (SDIM) [17]. The results of this model test showed the strong real-time performance of the 1D CNN-based SDIM. In a follow-up study, Avci et al. proposed an entirely new scheme that applies 1D CNNs for SDD under real-time environmental conditions in a wireless sensor network (WSN) SHM system [18,19]. Furthermore, the recognition ability of the model was also experimentally validated. Then, on the basis of the previous studies, Avci et al. and Abdeljaber et al. presented another enhanced SDIM based on a 1D CNN architecture [20,21]. In this work, the feasibility of 1D CNN-based SDIM was further validated using the data of structural health monitoring benchmark model proposed by The International Association for Structural Control and The American Society of Civil Engineers (IASC-ASCE). More recently, Sharma et al. utilized the output-only structural response data of a semi-rigid frame structure to build a 1D CNN-based model to identify joint damage conditions. In addition, the impact of ambient noise contamination levels on the recognition accuracy of the model was included in the analysis. The results suggested that the 1D CNN-based SDIM performed well with high accuracy and robustness.

Currently, most current research objects in the field of SHM/SDD are primarily large-scale frame structures, while the high-pile wharfs in port engineering have unique structural dynamic characteristics compared with these structures. Particularly, it is stressed that the structural capacity of high-pile wharfs is highly sensitive to structural damage. However, thus far, no research on the SDD of high-pile wharfs using 1D CNNs has been conducted. Although 1D CNNs have been proven to be feasible methods for current vibration-based global SDD applications to large-scale framework structures, with respect to high-pile wharfs, in-depth investigations on the real-time identification performance of SDIMs based on 1D CNNs have not been reported. Therefore, introducing 1D CNNs with strong automatic engineering capabilities to the SHM of high-pile wharfs offers promising prospects.

2. Research significance and objectives

Due to the lack of efficient and economical real-time SHM systems, the global structural damage of the high-pile wharfs generated in harsh marine environments is difficult to monitor in a timely manner, which poses an enormous threat to the safety of workers and property. 1D CNNs have been proven to be feasible methods for current vibration-based global SDD applications to large-scale framework structures; however, with respect to high-pile wharfs, in-depth investigations on the real-time identification performance of SDIMs based on 1D CNNs have not been reported at present. Therefore, introducing 1D CNNs with strong automatic engineering capabilities to the SHM of high-pile wharfs has broad prospects. The present research was conducted to satisfy three main objectives: (i) establishing a method framework based on 1D CNNs and FEM to realize the intelligent identification of the overall

structural damage of high-pile wharfs; (ii) exploring the performance differences (using the correct recognition rate) between the DL models trained by two distinct classes of datasets and (iii) verifying the directional sensitivity of the intelligent model to the displacement responses of typical high-pile wharfs, further optimizing the acquisition strategy of structural damage dynamic response data under limited sensor conditions.

3. Methodology

The proposed 1D CNNs based methodology is established within a data-driven vibration-based structural health monitoring (VSHM) framework for supervised learning similar to the case described in literature. The methodology is divided into five steps: (i) to select possible and/or typical damaged scenarios of the monitored structure (i.e. single damaged pile at specific location of the independent structural segment of the high-pile wharf); (ii) FE models were built for all possible damaged scenarios, including the undamaged scenario, in which structural damage was introduced in terms of stiffness reduction of the specific single pile; (iii) to maximize the validity of FE models by minimizing the variances of first 3 orders of modal shapes and frequencies between prototype structure and the undamaged FE model; (iv) performing transient dynamics calculations for all damaged and undamaged scenarios under a sudden unloading and recording multi-point dynamic time history responses. The serial number of scenarios serves as a label for these responses; (v) establish a 1D CNNs model to learns the nonlinear relationship between the multi-point dynamic time history responses and their corresponding serial number of scenarios. This model is used to predict the damaged scenario of multi-point dynamic time history responses observed by new monitoring conditions. The five steps of the methodology will be illustrated more in detail in the following sections.

Consider a high-pile wharf equipped with a total n displacement transducer that measure the multi-point vibration responses. Once total of m damaged scenarios is determined as following:

$$\boldsymbol{DS} = [\boldsymbol{U}_0, \boldsymbol{D}_1, \boldsymbol{D}_2, \cdots \boldsymbol{D}_{\boldsymbol{m}-1}] \tag{1}$$

where $\boldsymbol{DS}$ denote damaged scenarios. The terms U_0 and D_i represent the structural intact state and damaged scenarios with stiffness reduction at pile $i^{\#}$ respectively.

The first set of the required data are the first 3 mode shapes and modal frequencies. These parameters could be calculated based on the recorded displacement time history responses at the top of pile foundations when the structure is intact (reference state). While the second data set used to train the 1D CNNs is generated by the FE models of all damaged scenarios (including undamaged scenario). The first 3 mode shapes and modal frequencies of prototype structure and FE model of intact structure (U_0 scenario) could be represented as:

$$\Phi_p = [\varphi_p^{(1)}, \varphi_p^{(2)}, \varphi_p^{(3)}] \tag{2}$$

$$\Phi_{FEM} = [\varphi_{FEM}^{(1)}, \varphi_{FEM}^{(2)}, \varphi_{FEM}^{(3)}] \tag{3}$$

$$F_p = [f_p^{(1)}, f_p^{(2)}, f_p^{(3)}] \tag{4}$$

$$F_{FEM} = [f_{FEM}^{(1)}, f_{FEM}^{(2)}, f_{FEM}^{(3)}] \tag{5}$$

where Φ_p, F_p and Φ_{FEM}, F_{FEM} denote the first 3 mode shapes and modal frequencies of the prototype structure and FE model of intact monitored structure respectively. While the terms $\varphi_p^{(i)}, \varphi_{FEM}^{(i)}$ and $f_p^{(i)}, f_{FEM}^{(i)}$ represent the ***ith***-order mode shapes and natural frequency of prototype structure and FE model of intact monitored structure respectively. It should be noted that there is a consistent one-to-one match between total $\boldsymbol{n}$ displacement transducers mounted on the structure and sampling points of the FE model of intact structure.

In engineering practice, the disturbance of environmental and optional variabilities (EOVs) will impact the accuracy of mode shapes of monitored structure in vibration measurement. In order to attenuate the effects of EOVs on the vibration responses of the prototype structure, only qualitative constraint for mode shapes is established in the proposed methodology:

$$\Phi_p \sim \Phi_{FEM} \tag{6}$$

where the symbol $\sim$ represents the similarity operator, which means only the consistency of general morphological characteristics of mode shapes between prototype structure and the FE model was required. For example, if the prototype structure's first 3 mode shapes are lateral, longitudinal and plane torsional mode, the FE model's corresponding mode shapes were required to be the same.

The quantitative constraint for first 3 modal frequencies of the optimized FE model can be described as follows:

$$\begin{cases} d^k\left(F_{FEM}^{(k)}, F_p\right) = \sqrt{\left(F_{FEM}^{(k)} - F_p\right)^T \left(\sum_{\psi}\right)^{-1} \left(F_{FEM}^{(k)} - F_p\right)} \\ d^k\left(F_{FEM}^{(k)}, F_p\right). < \epsilon \end{cases} \tag{7}$$

where $d^k\left(F_{FEM}^{(k)}, F_p\right)$ represents the Mahalanobis Distance (MD) between the first 3 modal frequencies vector of prototype structure and

FE model $\boldsymbol{k}^{\#}$ of intact monitored structure. While the $\sum_{\psi}$ is the covariance between the potential optimized FE models of intact monitored structure in search space ψ. It should be noted that multiple influence factors such as monitoring precision, structural characteristics and hardware facility are required to be considered comprehensively when determining the specific value of tolerance ϵ.

Once the optimized FE model of intact monitored structure, namely benchmark model, which is confirmed by constraints of equations of (6) and (7) has been determined, the next step is to establish total $\boldsymbol{m}$ FE models for all damaged scenarios ($\boldsymbol{DS}$) based on this benchmark model. For example, if the damaged scenario $\boldsymbol{i}^{\#}$ indicated that stiffness reduction was occurred at pile $\boldsymbol{i}^{\#}$, the FE model $\boldsymbol{i}^{\#}$ was established through introducing stiffness reduction at pile $\boldsymbol{i}^{\#}$ of the benchmark model while the rest components remain the same.

The dynamic responses obtained by the transient dynamic calculations of all FE models representing different damaged scenarios can be shown as follows, it should be noted that all damaged scenarios are under the same dynamic excitation (impact loading and sudden unloading).

$$\begin{cases} \boldsymbol{U}_0 = \left[U_0, U_{\Delta t}, U_{2\Delta t}, \cdots, U_{t_0}\right]^T \\ \boldsymbol{D_i} = \left[D_0^{(i)}, D_{\Delta t}^{(i)}, D_{2\Delta t}^{(i)}, \cdots, D_{t_0}^{(i)}\right]^T \end{cases} \tag{8}$$

where $\boldsymbol{U}_0$ and $\boldsymbol{D_i}$ denote the results of transient dynamic calculations for the undamaged scenario and damaged scenario $\boldsymbol{i}^{\#}$, respectively. The terms $U_{\Delta t}$ and $D_{\Delta t}^{(i)}$ represent the calculated multi-point dynamic responses at time step Δt for the undamaged scenario and damaged scenario $\boldsymbol{i}^{\#}$, respectively. The subscript t_0 denotes the timespan of transient dynamic computation.

Assuming that each calculated single-point dynamic response at sampling point $\boldsymbol{s}^{\#}$ ($\mathbf{s} \le n | \mathbf{s} \in \mathbb{N}$) consists of n_l samples ($n_l = t_0/\Delta t$), the next step is to align $\boldsymbol{n}$ single-point dynamic responses acquired at total n sampling points in time steps as follows:

$$\boldsymbol{U}_0 = \begin{bmatrix} U_{1,0} & U_{2,0} & \cdots & U_{n,0} \\ U_{1,\Delta t} & U_{2,\Delta t} & \cdots & U_{n,\Delta t} \\ \vdots & \vdots & \ddots & \vdots \\ U_{1,t_0} & U_{2,t_0} & \cdots & U_{n,t_0} \end{bmatrix}_{n_l \times n} \quad \boldsymbol{D_i} = \begin{bmatrix} D_{1,0}^{(i)} & D_{2,0}^{(i)} & \cdots & D_{n,0}^{(i)} \\ D_{1,\Delta t}^{(i)} & D_{2,\Delta t}^{(i)} & \cdots & D_{n,\Delta t}^{(i)} \\ \vdots & \vdots & \ddots & \vdots \\ D_{1,t_0}^{(i)} & D_{2,t_0}^{(i)} & \cdots & D_{n,t_0}^{(i)} \end{bmatrix}_{n_l \times n} \tag{9}$$

where the term $U_{i,j} \epsilon \boldsymbol{U}_0$ ($0 \le i \le n, 0 \le j \le n_l | i,j \in \mathbb{N}$) represent the output displacement of sample $\boldsymbol{i}^{\#}$ point at time step $\boldsymbol{j}^{\#}$ for the undamaged scenario. While the term $D_{j,k}^{(i)} \epsilon \boldsymbol{D_i}$ ($0 \le i < m, 0 \le j \le n, 0 \le k \le n_l | i,j,k \in \mathbb{N}$) is the output displacement of sample point $\boldsymbol{j}^{\#}$ at time step $\boldsymbol{k}^{\#}$ for the damaged scenario $\boldsymbol{i}^{\#}$.

The next step is to train the 1D CNNs. Each frame (row) in $\boldsymbol{U}_0$ and $\boldsymbol{D_i}$ is labeled by the corresponding damaged scenario serial number. For example, in the damaged scenario $\boldsymbol{i}^{\#}$, total n_l rows $\epsilon \boldsymbol{D_i}$ are labeled as category $\boldsymbol{i}$ **;** then the frames are normalized in the interval $(-1, 1)$. The data can be represented as:

$$\begin{aligned} \boldsymbol{U}_0 &= \begin{bmatrix} NU_{1,0} & NU_{2,0} & \cdots & NU_{n,0} & 0 \\ NU_{1,\Delta t} & NU_{2,\Delta t} & \cdots & NU_{n,\Delta t} & 0 \\ \vdots & \vdots & \ddots & \vdots & 0 \\ NU_{1,t_0} & NU_{2,t_0} & \cdots & NU_{n,t_0} & 0 \end{bmatrix}_{n_l \times n} \\ \boldsymbol{D_i} &= \begin{bmatrix} ND_{1,0}^{(i)} & ND_{2,0}^{(i)} & \cdots & ND_{n,0}^{(i)} & i \\ ND_{1,\Delta t}^{(i)} & ND_{2,\Delta t}^{(i)} & \cdots & ND_{n,\Delta t}^{(i)} & i \\ \vdots & \vdots & \ddots & \vdots & i \\ ND_{1,t_0}^{(i)} & ND_{2,t_0}^{(i)} & \cdots & ND_{n,t_0}^{(i)} & i \end{bmatrix}_{n_l \times n} \end{aligned} \tag{10}$$

Total $m-1$ damaged ($\boldsymbol{D_i}$) and one benchmark ($\boldsymbol{U}_0$) datasets were then spliced along the vertical axis. It should be noted that the order within a dataset cannot be changed but the order between datasets can be arbitrarily arranged. This data fusion approach can effectively preserve the temporal resolution of the damage information within the data. The final dataset used to train the 1D CNNs based SDD model can be represented as follows:

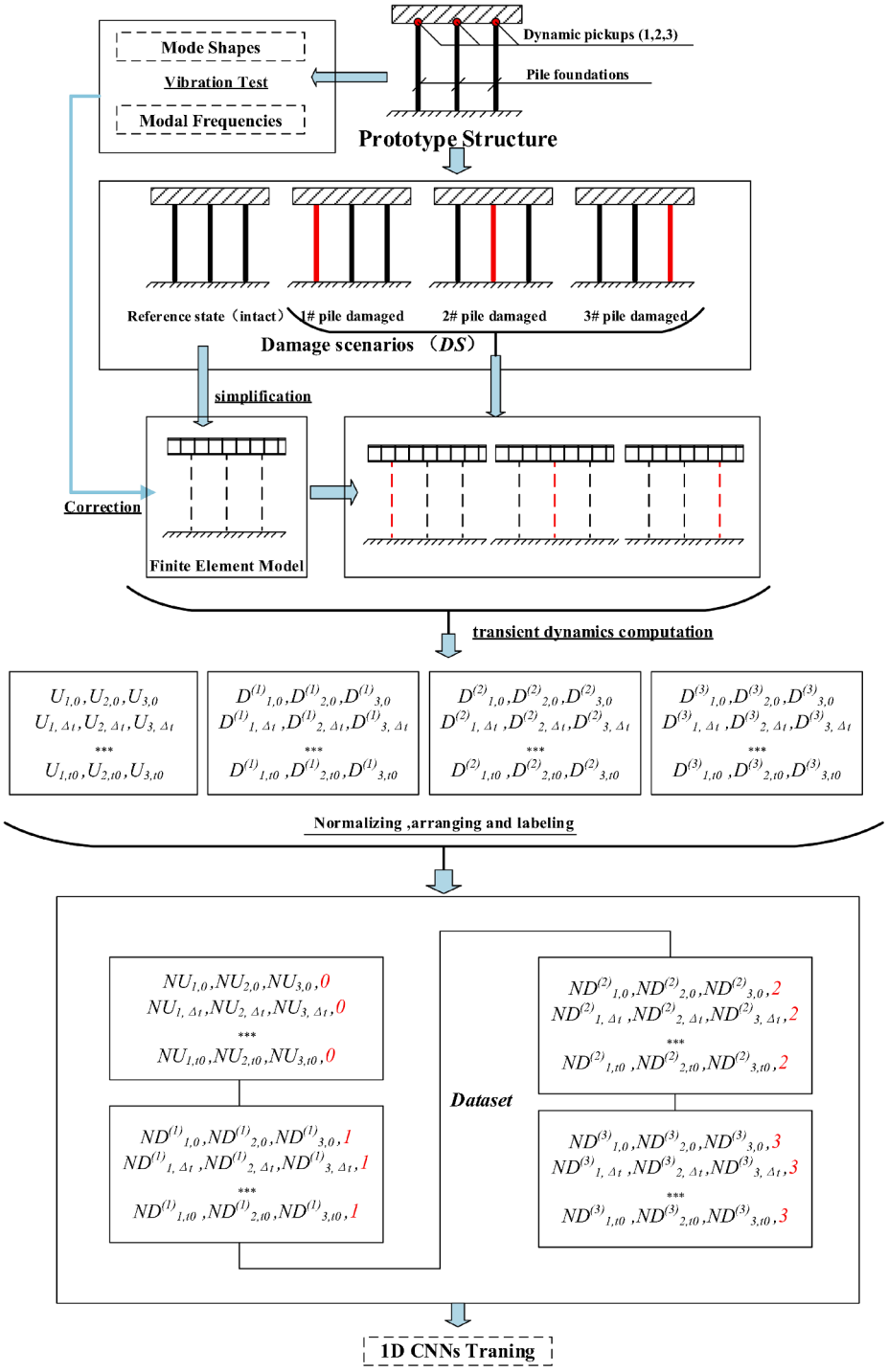

Fig. 1. Schematic diagram of the suggested methodology.

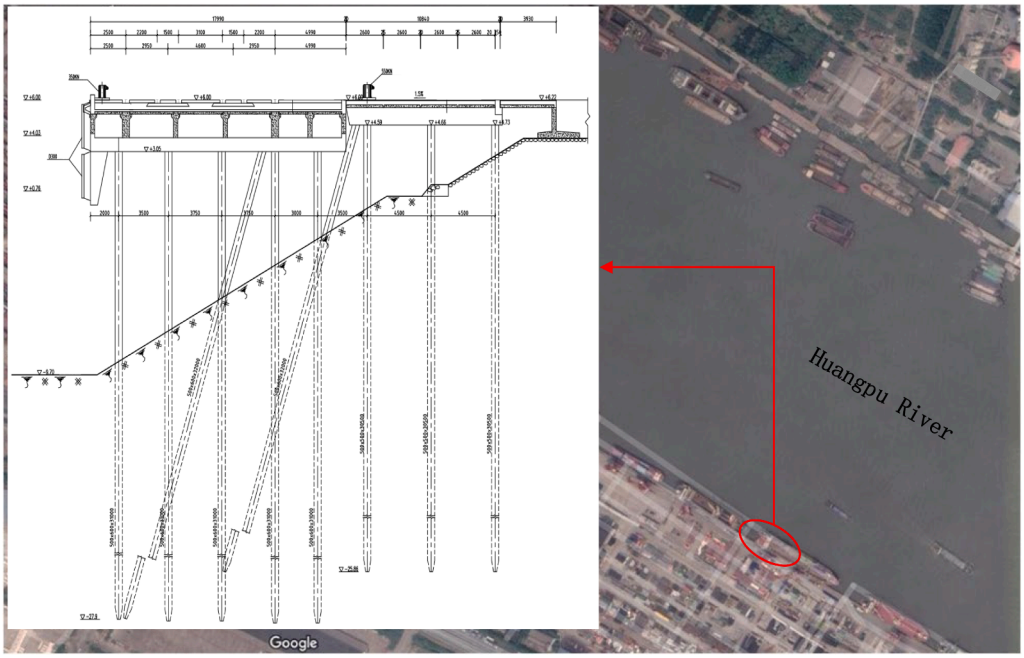

Fig. 2. Layout and cross-sectional diagram of the typical high-pile wharf in Shanghai Port.

$$dataset = \begin{bmatrix} NU_{1,0} & NU_{2,0} & \cdots & NU_{n,0} & 0 \\ NU_{1,\Delta t} & NU_{2,\Delta t} & \cdots & NU_{n,\Delta t} & 0 \\ \vdots & \vdots & \cdots & \vdots & 0 \\ NU_{1,t_0} & NU_{2,t_0} & \cdots & NU_{n,t_0} & 0 \\ ND_{1,0}^{(1)} & ND_{2,0}^{(1)} & \cdots & ND_{n,0}^{(1)} & 1 \\ ND_{1,\Delta t}^{(1)} & ND_{2,\Delta t}^{(1)} & \cdots & ND_{n,\Delta t}^{(1)} & 1 \\ \vdots & \vdots & \vdots & \vdots & \vdots \\ ND_{1,t_0-\Delta t}^{(m-1)} & ND_{2,t_0-\Delta t}^{(m-1)} & \cdots & ND_{n,t_0-\Delta t}^{(m-1)} & m-1 \\ ND_{1,t_0}^{(m-1)} & ND_{2,t_0}^{(m-1)} & \cdots & ND_{n,t_0}^{(m-1)} & m-1 \end{bmatrix}_{(n_t \times m) \times n} \tag{11}$$

Then, for the above generated dataset, back propagation (BP) algorism is used to train the 1D CNNs based SDD model. Once the training is completed, the model can classify any input frame of measured dynamic responses. Related algorithms during training process were described in detail in Appendix A. The schematic diagram of the suggested methodology which is applied for the planar-frame structures similar to pile-supported wharfs can be illustrated in Fig. 1.

4. Case studies

4.1. Geometric model

A beam-slab-type high-pile wharf located in Shanghai Port was chosen for this study. The overall structure is arranged alongshore with a longitudinal length of 128 m and a horizontal width of 26.7 m, and the layout and cross-sectional diagrams are shown in Fig. 2. The paper selected the independent structural sediment in the middle of the working area as the analysis object. It consisted of 7 lateral bends of which the spacing was 7 m, and each frame was composed of 5 vertical piles and 1 inclined pile. These pile foundations are all square piles with a side length of 600 mm. The main upper structure adopts inverted T-shaped beams and panels that are both made of cast-in-place reinforced concrete. The lower beam is 0.9 m wide and 0.8 m high, the upper beam is 0.4 m wide and 1.6 m high, the longitudinal beam is 0.4 m wide and 1.6 m high, and the plate thickness is 0.8 m.

To simplify the analysis, the interaction between piles and foundation soil was assumed to be fixed bonded instead of direct modeling in this study. Therefore, the “m” method was utilized to determine the calculated length of the piles to meet the equivalent lateral stiffness principle [22].

The “m” method assumes that the horizontal foundation resistance coefficient of soil increases linearly with the depth of soil,

Table 1
Summary of the calculation results of the relative depth of each pile bottom embedded point to the pile top based on the "m" method (mm).

Pile Number	1	2	3	4	5	6
Calculated Length (mm)	14,400	13,000	11,400	12,400	9800	8550

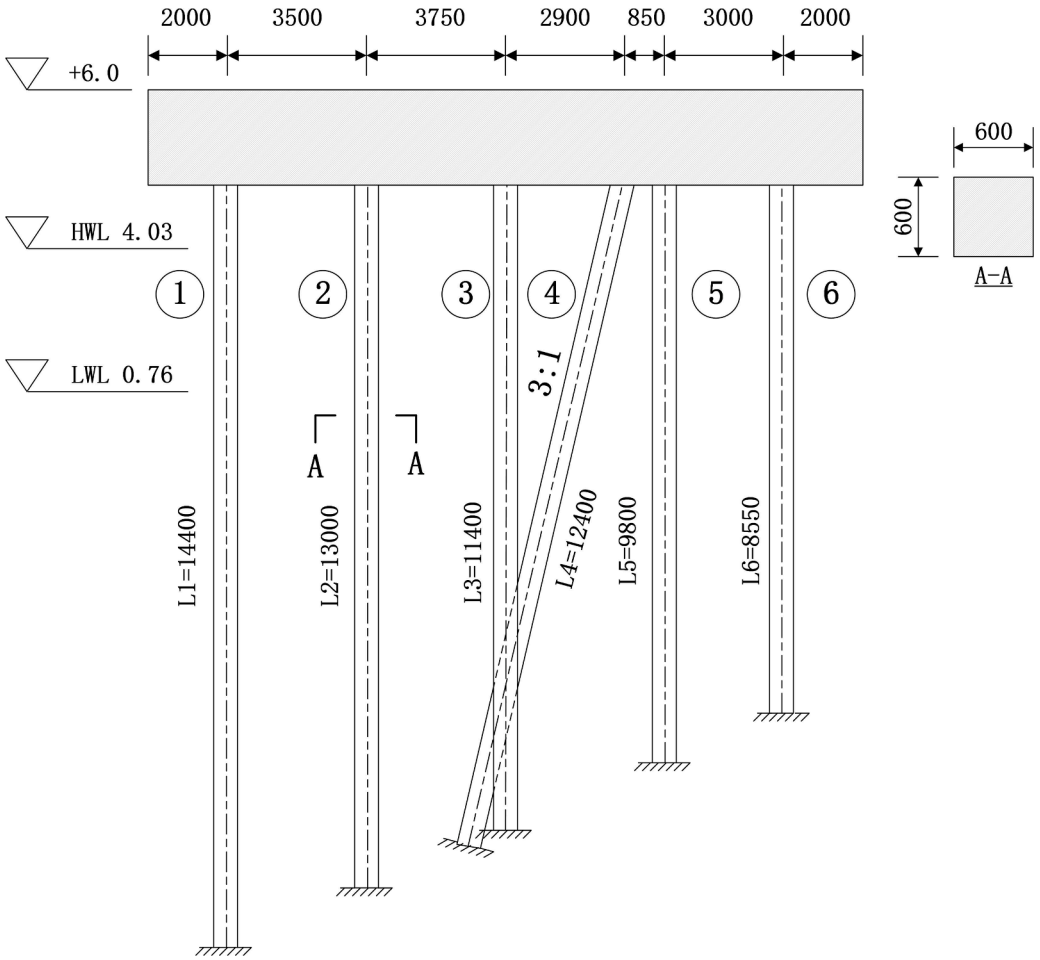

Fig. 3. Simplified calculation diagram of the bent structure section of a high-pile wharf based on the "m" method.

namely:

$$K = mz \tag{12}$$

where K denotes the horizontal foundation resistance coefficient of soil (kN/m^3), m is the proportional coefficient (kN/m^4), and z represents the depth of the calculated point (m).

Since the original foundation soil is distributed in layers, the m-value adopts the weighted average of m of each soil layer at a depth of 1.8 T below the ground:

$$T = \sqrt[5]{\frac{E_P I_P}{m b_0}} \tag{13}$$

where E_p indicates the modulus of elasticity of piles (kN/m^2), I_p is the cross-sectional moment of the inertia of piles (m^4), and b_0 is the converted width (m). b_0 is calculated as:

$$b_0 = k_f(1.5d + 0.5) \tag{14}$$

where k_f is the shape conversion factor of pile. Here, this value is set as 1.0, which results in $b_0 = 1.4(m)$.

The structural foundation square piles were prefabricated using C30 concrete, and the modulus of elasticity was 2.7×10^4 MPa.

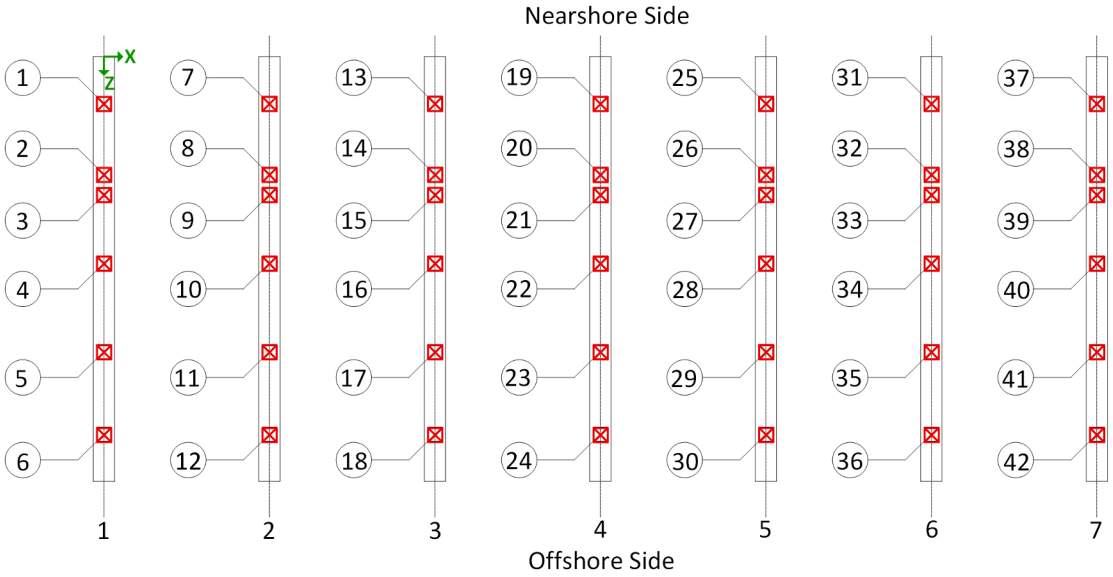

Fig. 4. Pile numbers of the selected structural sediment.

Table 2
Damage condition setting table.

Damage condition number	Number of pile with reduced stiffness
condition $0^{\#}$	none
condition $i^{\#}$	pile $i^{\#}$

Remark: i in Table 2 represents an integer from 1 to 42, which corresponds to the pile number in Fig. 4.

Moreover, the straight piles are 31 m long, the oblique piles are 32 m long, and the maximum depth of piles is 18.25 m. After weighted average calculation, $\mathrm{m} = 4500(\mathrm{kN/m^4})$. It can be further calculated that $T = 1.2(m)$.

The depth of the embedded point is calculated according to the following equation:

$$\mathrm{t} = \eta \mathrm{T} \tag{15}$$

where the empirical parameter η takes values ranging from 1.8 to 2.2. This study sets the parameter as 2.0, which results in $t = 2{*}1.2\mathrm{m} = 2.4(\mathrm{m})$

The calculated length of the foundation piles, which were obtained after substituting the structural dimensions of each pile into the above calculation methods, are listed in Table 1 as follows.

According to the above results, the calculation section of the typical high-pile wharf can be further simplified as shown in Fig. 3.

4.2. Structural damage scheme

The essence of structural damage can be defined as the loss of local stiffness in the damaged section [23]. When damage occurs, the lateral loading capacity of the pile will thus be determined by the residual effective stiffness of the damaged section. The overall damage rate ω can be defined as the ratio of the residual effective cross-sectional area $(\bar{A})$ of the damaged section to the original section (A) that is in the nondestructive state. It can be mathematically formulated as [24]:

$$\omega = \frac{A - \bar{A}}{A} = 1 - \frac{\bar{A}}{A} \tag{16}$$

According to the strain equivalence and Saint-Venant principles, the elastic modulus of the damaged pile foundation is:

$$\bar{E} = (1 - \omega){*}E \tag{17}$$

The structural sediment selected by this research has a total of 42 foundation piles, which were numbered sequentially from the top left to the bottom right of the structural floor plan, as shown in Fig. 4.

Each damaged pile in different locations was set as a single damage condition based on the idea of orthogonal experiments, which

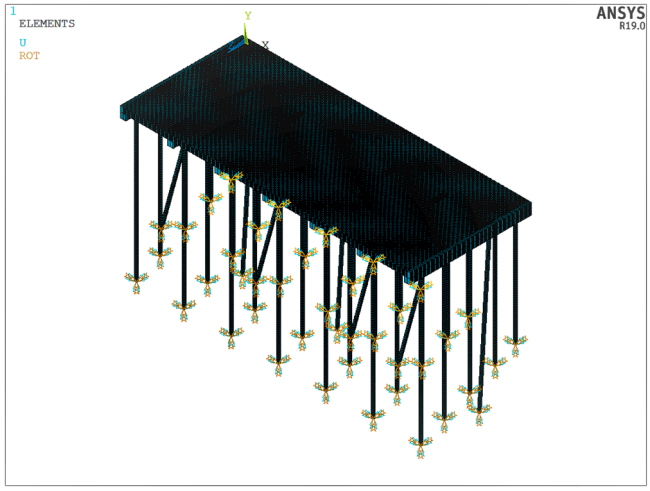

Fig. 5. Fixed constraints on pile bottom.

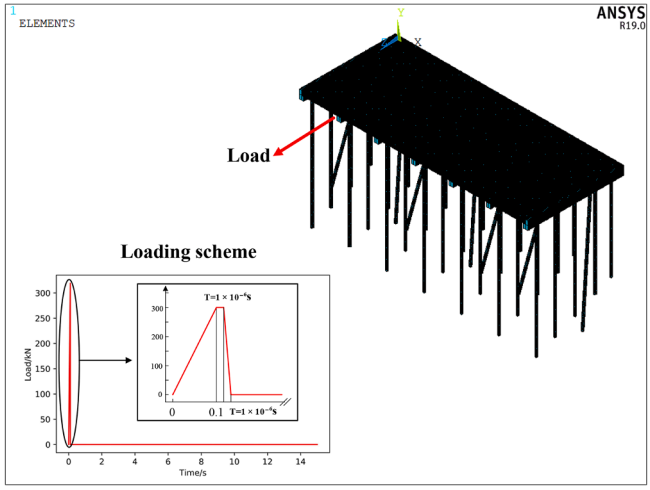

Fig. 6. Loading scheme.

resulted in a total of 42 scenarios. Besides, the scenario where all piles are undamaged is also considered. The settings of the damage conditions are presented below in Table 2.

As shown in Table 2, condition $0^{\#}$ means that none of the piles have reduced stiffness, and the multipoint displacement dynamic response calculated by the finite element model in this condition is utilized as the basic structural response vector in the healthy state. Similarly, condition $i^{\#}$ means that pile $i^{\#}$ has its stiffness reduced 50% to simulate the global stiffness degradation induced by structural damage. It must be emphasized that taking different degrees of stiffness loss within a certain range to simulate real structural damage will not have a fundamental impact on the proposed method in this study.

4.3. Finite element model simulation

In this paper, the 3D finite element model of the structural sediment of a high-pile wharf was built in ANSYS 19.0.

4.3.1. Boundary conditions

The interactions between pile foundations and soil were simplified, fixed constraints were imposed on the bottom of all pile foundations and the details are presented in Fig. 5. This study utilized sudden unloading loads to excite the structure and selected the end node of the second bent frame on the west side as the loading point. The entire loading scheme is shown in Fig. 6. Briefly, the loading scheme is divided into 4 steps. In the first step, the loads increase from 0 to 319.3 KN within 0.1 s. In the second step, the loads are maintained constant, and the duration is only 1×10^{-6}s. This is done to fulfill the convergence criteria of numerical calculations

Table 3
First 10 orders of natural frequencies of the finite element model.

Order	Natural frequency/Hz	Order	Natural frequency/Hz
1	1.002	6	2.285
2	1.244	7	2.285
3	1.283	8	2.286
4	2.284	9	2.286
5	2.284	10	2.286

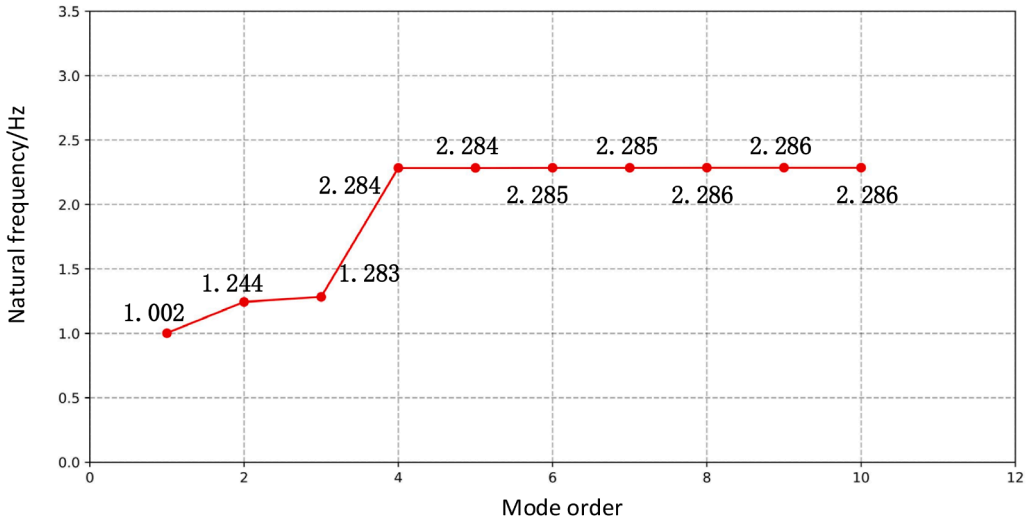

Fig. 7. Distributions of the first 10 orders of natural frequencies.

Table 4
Comparison of the first three orders of natural frequencies of the high-pile wharf structure.

Study/natural frequency	First order	Second order	Third order
Boroscheket et al [27]	1.023	1.432	1.654
Cheng et al [28]	0.698	1.084	1.182
This article	1.002	1.244	1.283

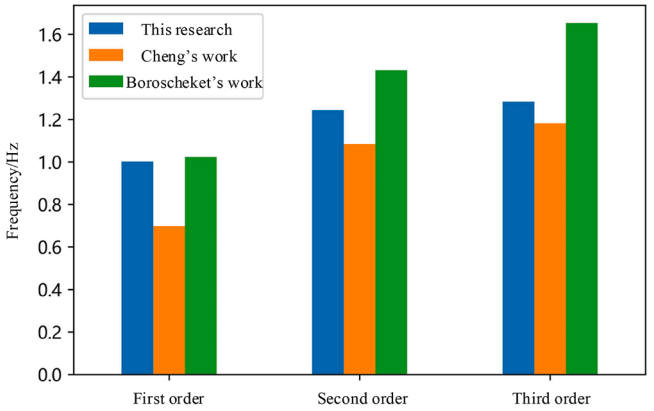

Fig. 8. Comparison of the vibration test frequency between the finite element model and similar prototype structure.

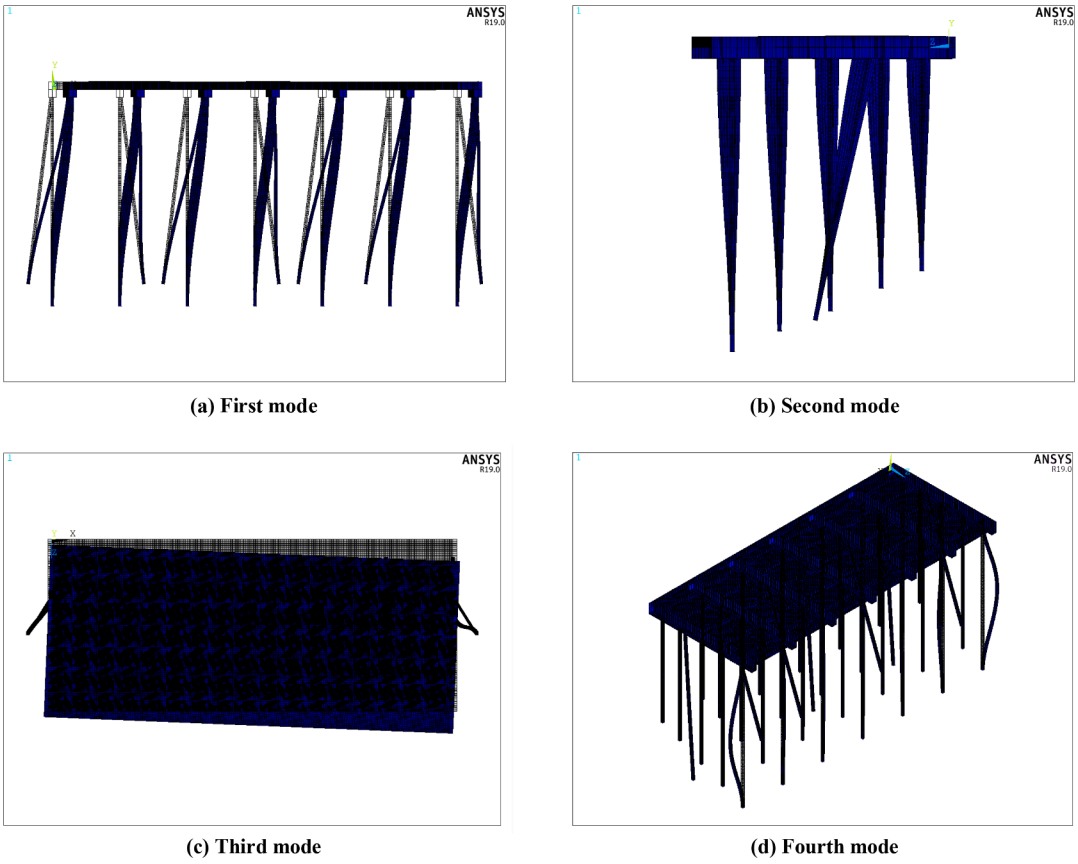

Fig. 9. The first four modes of vibration of the typical high-pile wharf.

Table 5
GCI index under different grid resolution schemes.

Average grid length/cm	25	50	75	100	125
GCI (%)	2.6	3.1	3.7	4.2	6.8

that replace the instant of unloading with a transient time step. Next, the duration is also set to 1×10^{-6} s in the third step, where the loads reduce to zero rapidly. Finally, the fourth step lasts 15 s, and there is no load on the structure section.

4.3.2. Dynamic characteristics verification

The first 10 orders of natural frequencies and their distributions of the finite element model are listed in Table 3 and Fig. 7, respectively.

It follows that the distribution of the first 10 orders of natural frequencies indicates a relatively obvious two-stage feature. The natural frequencies are slightly increased in the first three order modes, and there is an apparent jump between the third and fourth orders. Additionally, the natural frequencies of higher-order modes are approximately equal. Collectively, this reflects the dynamic characteristics of the structure from simple global vibration to complex local vibration.

In 2010, Boroscheket et al. conducted a vibration test on a high-pile wharf at the harbor of Ventanas (Chile) and successfully collected the first three orders of natural vibration frequencies of the structure [25]. Later, in 2011, Cheng et al. measured the vibration of a high-pile wharf under ambient excitation in three periods during high water, low water, and between the two levels and obtained the corresponding data of the structure [26]. The contrasts between our numerical calculation results of the natural frequencies and those derived from the former two studies are listed in Table 4 and Fig. 8. The table and figure show that the finite element model established in this paper can accurately reflect the natural frequency distribution characteristics of the actual structure.

Regarding the modes, the results show that the first three modes of the high-pile wharf structure are respectively manifested as the overall longitudinal vibration, overall transverse vibration, and overall torsional vibration while the fourth and higher modes are mainly represented as independent local vibration, as shown in Fig. 9. The fifth to tenth order structural modes are shown in Appendix B.

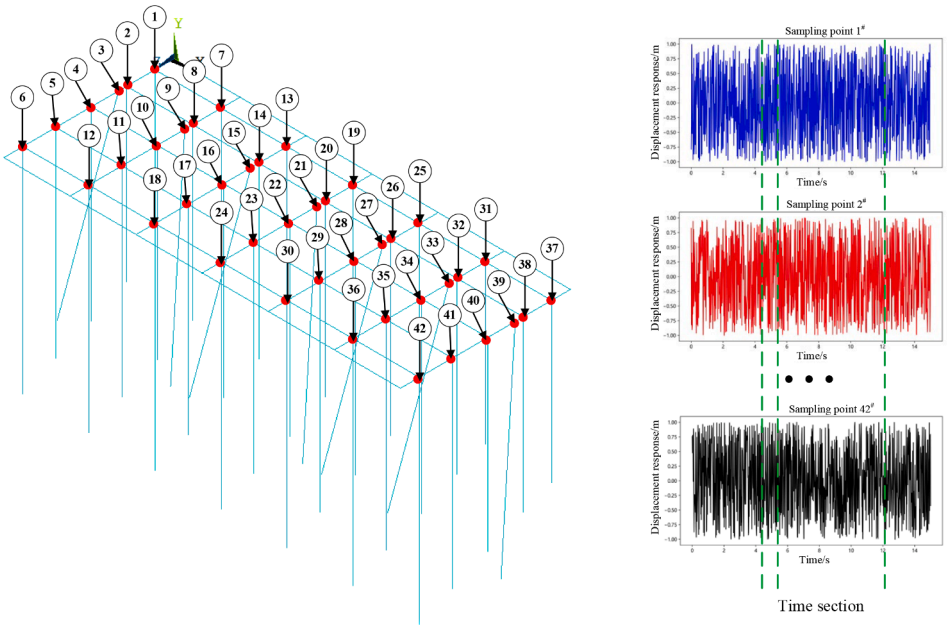

Fig. 10. Locations of the sampling points.

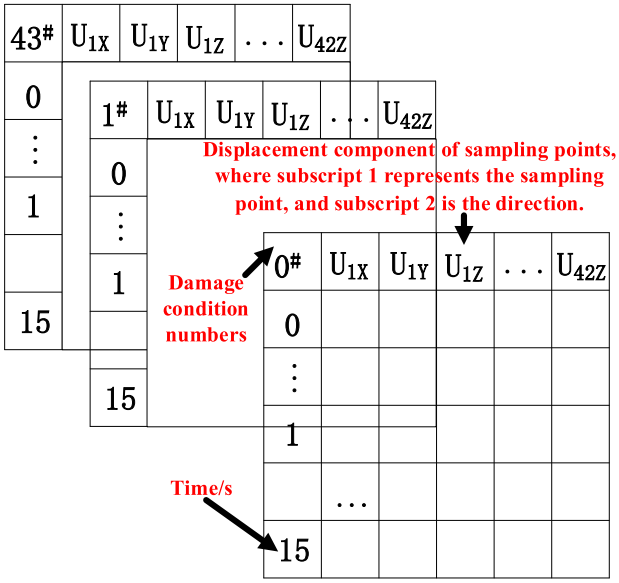

Fig. 11. Data structure of the multipoint displacement response under all working conditions.

Taken together, the dynamic characteristics of the established FE model are highly consistent with the field test. Therefore, the FE model established in this paper for the selected high-pile wharf structure section is reliable and valid.

4.3.3. Grid resolution analysis

This study introduced the grid convergence index (GCI) to quantitatively evaluate the uncertainty of the calculation results [27]. Five different grid resolutions, denoted S1, S2, S3, S4, S5, with mesh lengths of 25 mm, 50 mm, 75 mm, 100 mm, and 125 mm, respectively, were utilized to analyze the established FE model. Table 5 summarizes the GCI of the FE model under different grid resolution schemes. As described in Table 5, the GCI increases with increasing average grid length. However, the GCI increases at a faster rate immediately after the grid size exceeds 100 mm. According to prior experience in FE calculation cases in the field of civil engineering, the GCI corresponding to the grid resolution of 100 mm meets the demand of calculation accuracy. Taken together, the grid resolution of 100 mm is used in this research to perform the transient dynamics calculation of the FE model.

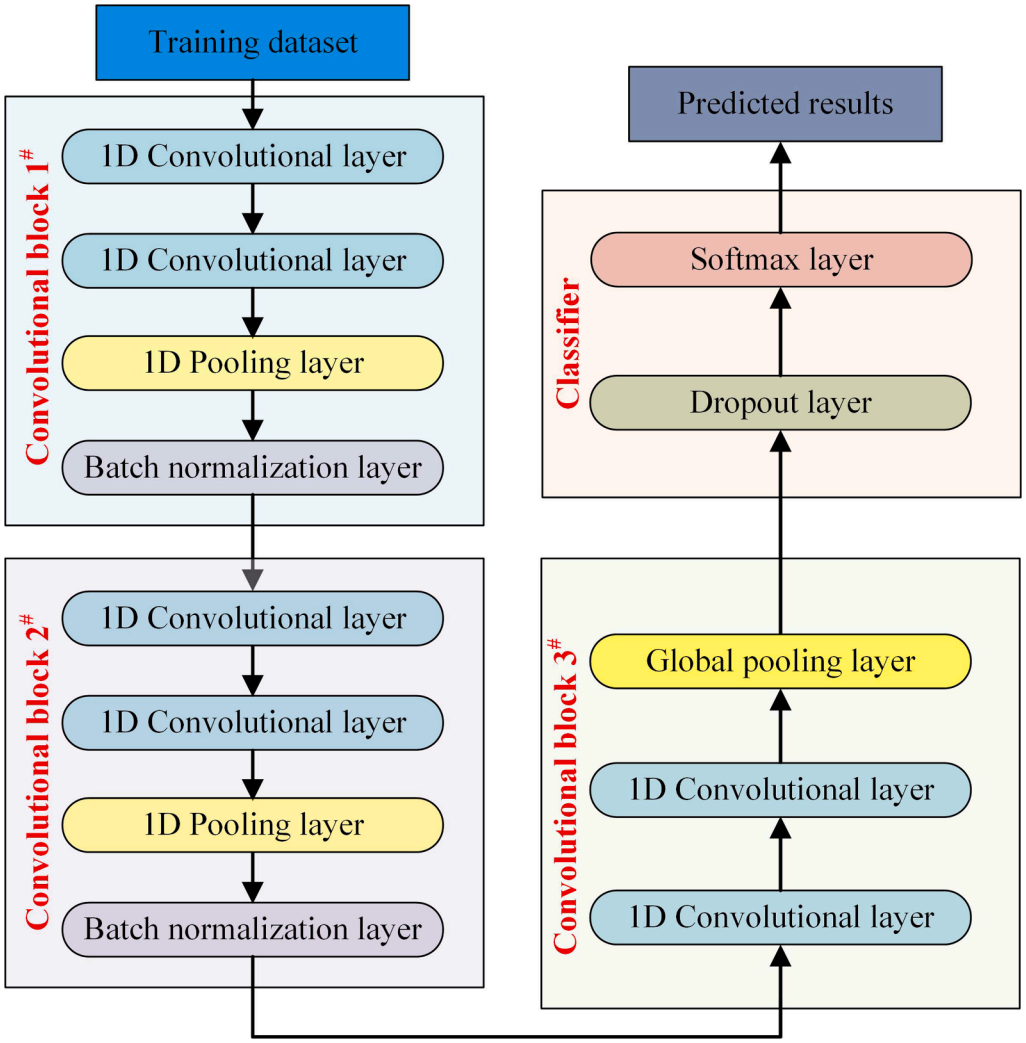

Fig. 12. Model architecture of the proposed CNNs.

4.3.4. Sampling scheme

The locations of the sampling points used to collect the displacement response, which are shown as red dots in Fig. 10, are selected as the 42 beam-pile nodes of the structural sediment where the measured dynamic response contains richer global damage information. The transient dynamics calculation process produced a total of 2494 results of all calculation substeps. Each substep outputs the displacement response time history of all sampling points in the three main axis directions (X, Y, and Z respectively representing the longitudinal, vertical and lateral directions of the high-pile wharf structure section). The data structure of the multipoint displacement response under all 43 groups of working conditions is demonstrated in Fig. 11.

All raw data in this section are available for download from GitHub at https://github.com/yujuezhou/Nonparametric-Vibration-Based-Damage-Detection-Framework-for-High-Pile-Wharf-Foundations.

5. Overview of one-dimension convolutional network

As a kind of multilayer feed-forward ANN, the CNN, a powerful computational model, is biologically inspired by the primary visual cortex and designed to mimic the receptive field of neurons [28,29]. Conventional 2D CNNs have been widely used to process two-dimensional data, such as images and videos. Different from 2D CNNs in which feature maps and kernels both use a 2D matrix, 1D CNNs, a modified version of the former, have been proven to be more suitable for processing 1D arrays, such as dynamic response signals. Overall, the multiple obvious advantages of 1D CNNs are summarized as follows [30]: (i) 1D CNNs have a more compact structure with fewer hidden layers and neurons, and the remarkable end-to-end characteristics facilitate the network's actual deployment; (II) unlike 2D CNNs using matrices, the computation complexity of 1D CNNs is significantly lower, mainly attributed to utilizing array operations in the forward propagation (FP) and backpropagation (BP), which highly improves calculation efficiency;

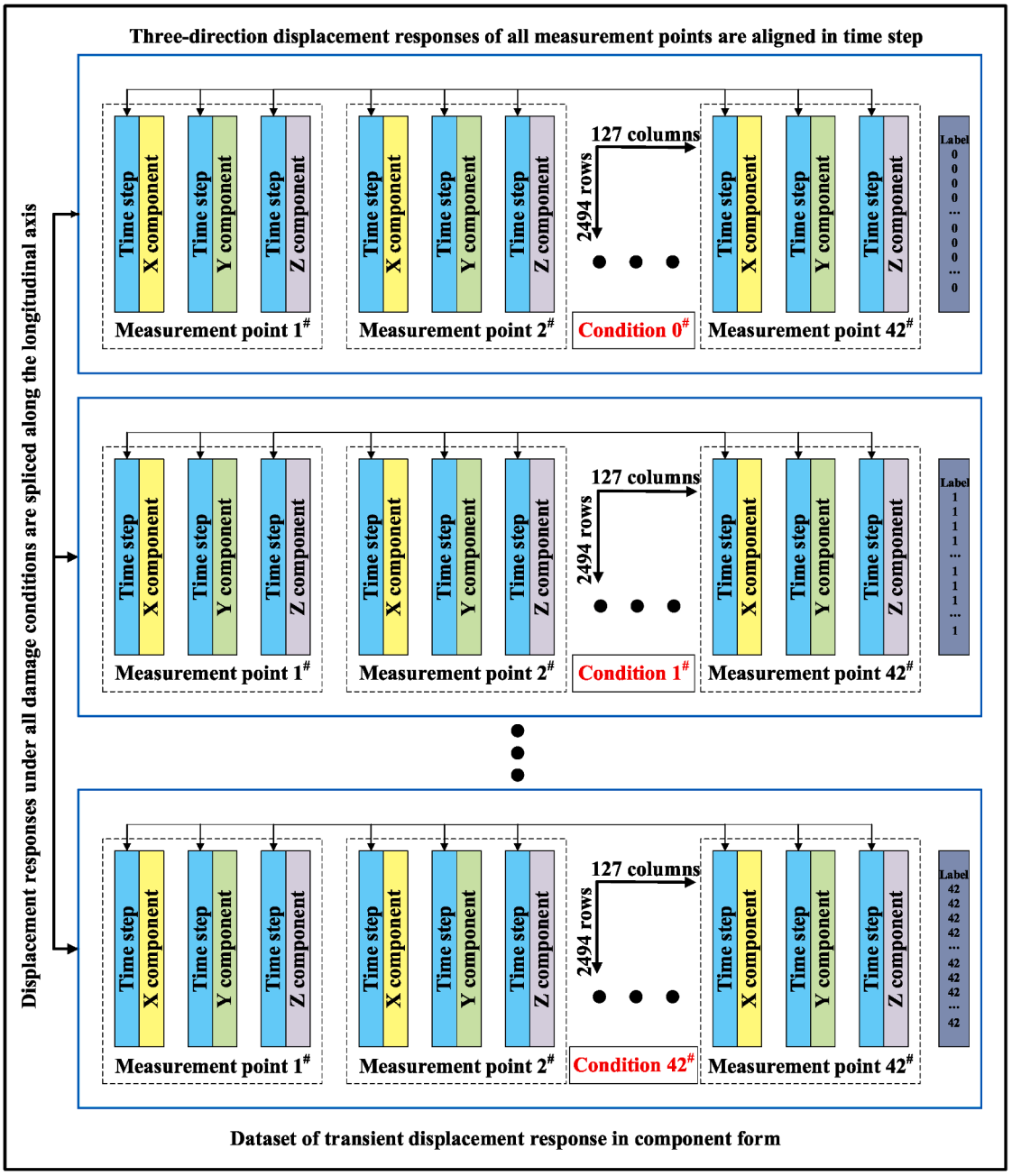

Fig. 13. Construction process of the component form dataset of transient displacement response.

(III) 1D CNNs can achieve a high level of detection accuracy under the minimum sized data set, while limited data sets can lead to overfitting problems for 2D CNNs; and (IV) 1D CNNs have lower sensitivity to the degree of translation, scaling, skewing and distortion of input data.

It is important to note that the learning process of CNNs is mainly divided into two steps: the FP process and the BP process. The former calculates the input data layer by layer; and the latter performs layer-by-layer weight adjustment to reduce the loss value, namely, the difference between the final output and the desired output. In addition, the two aforementioned processes are repeated until the learning of CNNs is completed.

The calculation processes of FP and BP are briefly described in Appendix A.

Table 6
Setup of the training groups.

Group number	Direction of displacement response		
	Longitudinal (X) direction	Vertical (Y) direction	Transverse (Z) direction
1	●		
2		●	
3			●
4	●	●	
5		●	●
6	●		●

6. The proposed damage detection framework

6.1. One-dimension CNNs overall architecture

The proposed 1D CNN architecture in this paper contains 12 hidden layers, specifically, 6 1D convolutional layers, 2 local pooling layers, 2 batch normalization layers, 1 global pooling layer and 1 random deactivation (dropout) layer. Among the layers, the batch normalization layers can avoid the vanishing gradient issue of multilayer networks by reconstructing the feature maps into a standard normal distribution with data transformation. Moreover, setting the dropout layer with a significant overfitting suppression capability can enhance the generalization capability of the entire model. Fig. 12 illustrates the model architecture.

6.2. Data preprocessing

In this study, two different types of transient displacement datasets, which are component form and absolute value form, were constructed to evaluate the performance differences of the CNN models learning from different forms of training sets.

(1) dataset in component form

For each damage condition, the displacement responses of all 42 beam-pile nodes in three directions were horizontally spliced according to the principle of time synchronization in this research. Next, we add a column along the end of the tensor as a label, and the content of the column is the current damage condition number i (i is an integer from 0 to 43). At this time, the displacement response data under each condition are formed in a 2D tensor format with dimensions of (2494, 127). Finally, the data of all damage conditions are vertically spliced according to the principle of measurement point alignment, and a 2D tensor D_c with dimensions of (107242, 127) is constructed. Fig. 13 gives a detailed description of the construction process of the component form dataset of the transient displacement response.

(2) dataset in absolute value form

Another dataset construction method is to take the norm of the vectors added in three directions at each beam-pile node as the displacement of the sampling points, which can be calculated using formula (18). Then, the labeling and refactoring process of the dataset is similar to the process of the former dataset. Therefore, the dataset of absolute value form is the 2D tensor D_s with dimensions of (107242, 43).

$$\|v_j^{(i)}\| = \sqrt[2]{\left(v_{j\_x}^{(i)}\right)^2 + \left(v_{j\_y}^{(i)}\right)^2 + \left(v_{j\_z}^{(i)}\right)^2} \tag{18}$$

where $\|v_j^{(i)}\|, v_{j\_x}^{(i)}, v_{j\_y}^{(i)}$, and $v_{j\_z}^{(i)}$ respectively represents the absolute value of the displacement and the longitudinal, vertical and lateral components of the displacement response at node $j^{\#}$ under the condition $i^{\#}$, respectively.

Each label item of 214,484 samples of the two types of training datasets, D_c and D_s, were all recoded as a 1D tensor with a dimension of (43,1) by the one-hot coding principle.

6.3. The training setup

Based on the idea of orthogonal experiments, this study established the following training strategies, as shown in Table 6. Briefly, in each training group, the population samples were randomly divided into 80%, 10% and 10%, as the training set, validation set, and testing set, respectively. In this study, the initial value of learning rate was 0.0001. As the training epochs proceeded, the learning rate was updated synchronously according to the exponential decay rate. The batch of the training sample is set as 128 and the upper limit of training epochs is 100. During the model training phase, we selected the early stopping method as the callback mechanism.

7. Results and discussions

7.1. Performance of stochastic benchmark model

To verify the feasibility of this DL model, a stochastic benchmark model based on random prediction is established to evaluate the efficiency of the proposed 1D CNNs in this paper.

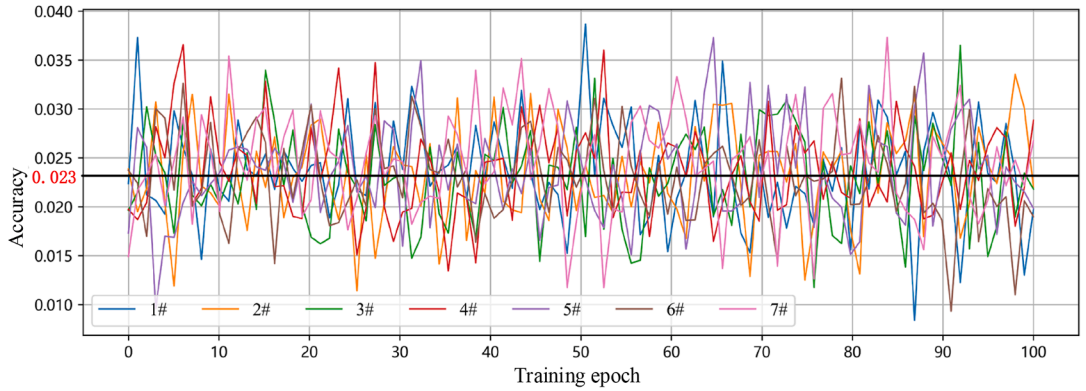

Fig. 14. Accuracy performance of stochastic benchmark model.

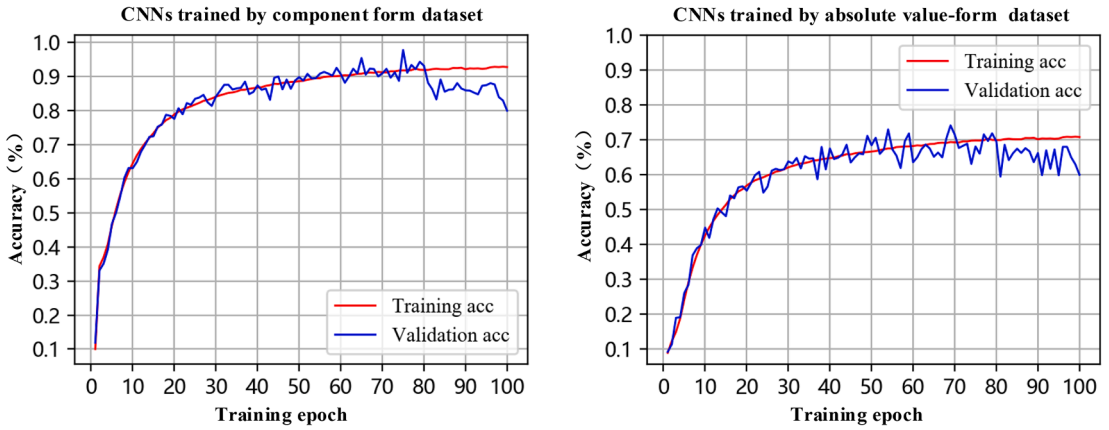

Fig. 15. Model performance of the 1D CNNs based on the two types of datasets.

There are a total of 43 different label categories in the damage conditions, and there are 2494 samples in each label category. Therefore, the SDD problem considered in this study is essentially a balanced multi-classification task. The true tag vector of each training group was compared with the predicted tag vector (a sequence of numbers with the same dimension as the tag vector) randomly generated by the benchmark model. The value of any component in the latter is an integer between 0 and 42. The above random process was performed 100 times for each training group, and the prediction accuracy was calculated as:

$$Accuracy = \frac{Count(T_i^{(j)} = P_i^{(j)})}{len(T^{(j)})} \tag{19}$$

where $T_i^{(j)}$ and $P_i^{(j)}$ respectively represent the value of the i th dimension in the true tag vector and the predicted tag vector of the j th training group, and both of them are integers between 0 and 42 ; $Count\left(T_i^{(j)} = P_i^{(j)}\right)$ denotes that the total number of true tags of the samples is equal to number of predicted tags in the j th training group; and $len(T^{(j)})$ is the dimensions of the true tag vector of the j th training group. The accuracy performance of the stochastic benchmark model is shown in Fig. 14.

The results of 1396,640 predictions revealed that the average accuracy rate of the stochastic benchmark model in the SDD classification task is approximately 0.023, which is roughly equivalent to the theoretical calculation value (0.02326); and the accuracy rate of any round in all training groups did not exceed 0.040. The underlying cause of this result is that the stochastic benchmark model essentially does not take advantage of any information related to the structural damage of the high-pile wharf. In other words, if the performance of the 1D CNNs is significantly better than that of the former, it can be concluded that through automatically learning of dynamic response signals, the model has acquired a certain degree of damage identification ability, namely, the DL-based algorithm does work indeed.

7.2. Impact of data format on model performance

The training accuracy and validation accuracy of the 1D CNN model based on two kinds of datasets, the component form and the absolute value form, are illustrated in Fig. 15.

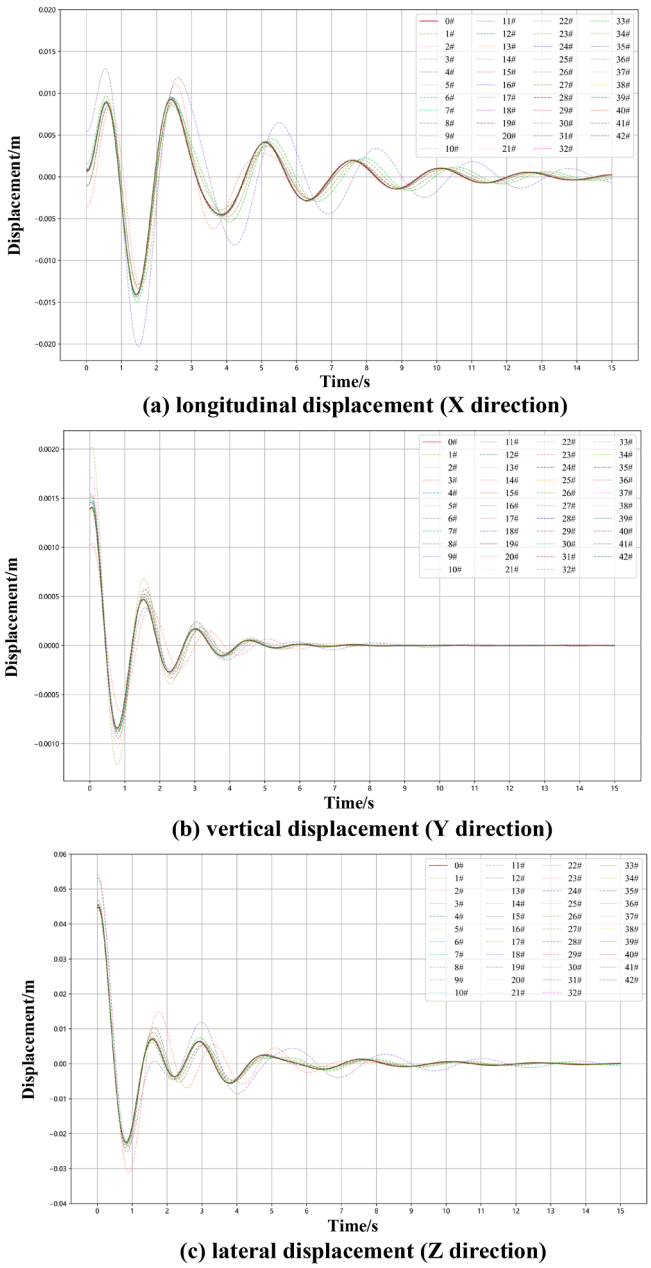

Fig. 16. Displacement responses of measurement point $1^{\#}$ in three main directions under 43 different working conditions.

Obviously, the above two models have both demonstrated superior recognition accuracy performance than the stochastic benchmark model over the course of 100 training epochs. The figure shows that in the first 20 training epochs, the training accuracy of the two models increased rapidly as the number of iterations increased. After more than 70 training epochs, the growth trend of the training accuracy is very slow and gradually levels off. Specifically the training accuracy of the CNNs based on the component form dataset (93.4%) is significantly higher than that of the model based on the absolute value form dataset (70.4%). Moreover, there is a certain degree of differences between the validation accuracy distribution of the two distinct models, which are specifically manifested as follows: (a) In the first 60 training epochs, the validation accuracy of the former model is less discrete and highly consistent with the trend of the training accuracy. Although the validation accuracy gradually deviates from the training performance during subsequent epochs due to overfitting problems generated by the model, the validation accuracy is still higher than the best level of the latter model. (b) The discreteness of the validation accuracy of the latter model is significantly higher than that of the former model; and it should be noted that more pronounced fluctuations have already appeared in the previous training epochs, which implies that the overfitting limits of this model are more prominent. The main reason for the above phenomena can be summarized as follows: the construction of

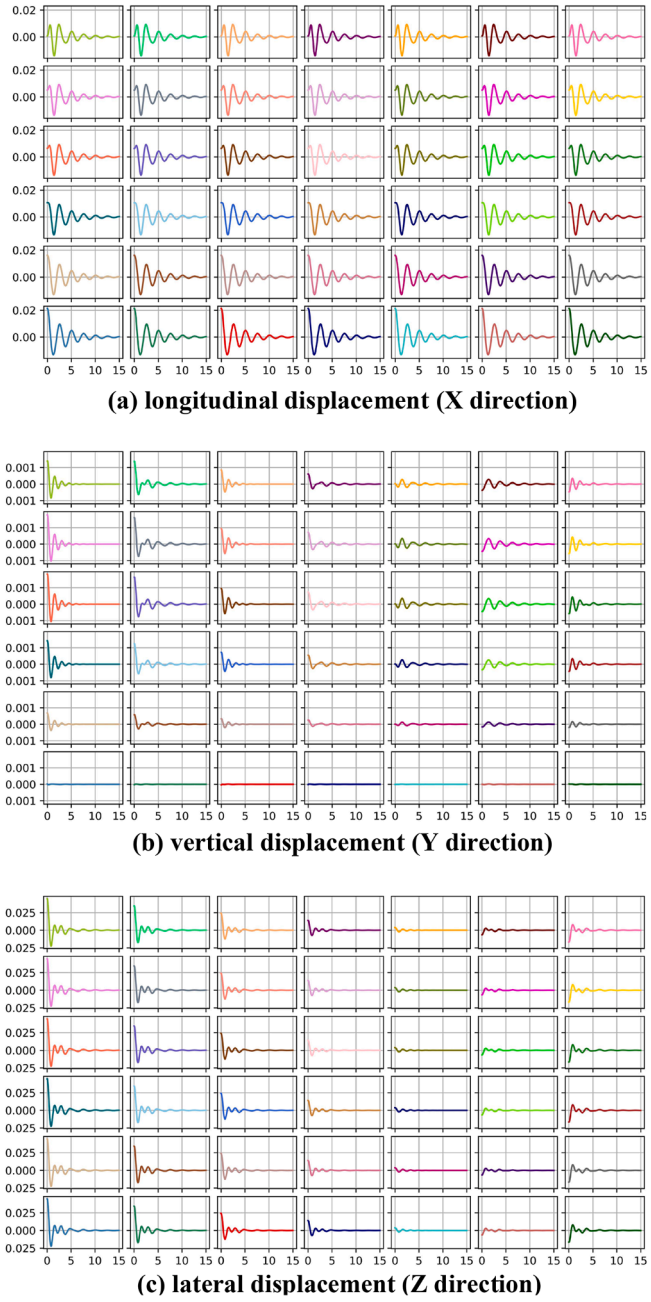

Fig. 17. Displacement responses of all 42 measurement points in three main directions under nondestructive conditions (damage condition $0^{\#}$).

an absolute value form dataset is essentially the condensation process of information (the large-scale compression of displacement response dimensions). This approach neglects the directional effect of global structural damage on the structural stiffness of pile foundations. Thus, this will inevitably result in the information loss of the local mode and make the DL model unable to fully perform its automatic engineering ability.

7.3. Directional sensitivity of the model to the displacement response

7.3.1. Time-domain characteristics of the displacement responses of the proposed FE model

To gain a comprehensive understanding of the internal rules, we acquired all displacement distributions of the specific measurement points under all 43 damage conditions and compared the displacement responses of all 42 measurement points under specific damage conditions. Due to space limitations, only the displacement responses of measurement point $1^{\#}$ under all working conditions

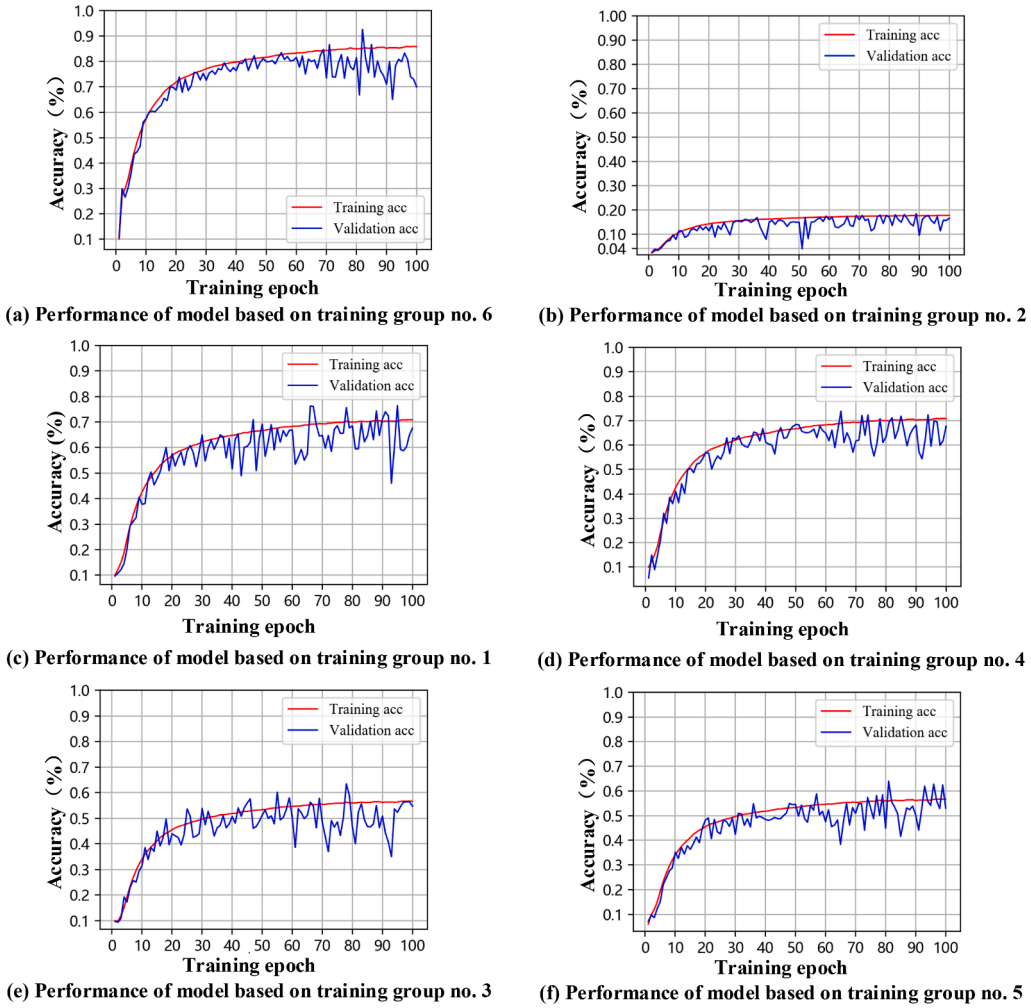

(a) Performance of model based on training group no. 6

(b) Performance of model based on training group no. 2

(c) Performance of model based on training group no. 1

(d) Performance of model based on training group no. 4

(e) Performance of model based on training group no. 3

(f) Performance of model based on training group no. 5

Fig. 18. Performance of the 1D CNN model based on 6 groups of reduced component displacement response datasets.

and the displacement responses of all measurement points under nondestructive working conditions are shown in Fig. 16 and Fig. 17. It needs to be emphasized that the relevant explanations in this section are based on the complete analysis of the related calculation results and are not only supported by a minimal amount of information in Fig. 16 and Fig. 17.

The displacement responses of all 42 measurement points under 43 damage conditions demonstrate the following: (a) For all measurement points, the displacement responses in the longitudinal and transverse directions (X direction and Z direction) are much larger than that in the vertical direction (Y direction). In addition, the phase difference of the longitudinal displacement response under different damage conditions is more discrete, and the longitudinal displacement response attenuation rate is the slowest; (b) The amplitude of the displacement of the measurement point will significantly increase when the corresponding pile is damaged. This phenomenon becomes more obvious when damage occurs at the location of the loading point (damage condition 12#); (c) The influence of the damaged pile on the displacement amplitude of the neighboring measurement point decreases as the plane distance increases. Besides, the effect of the damaged offshore pile on the overall displacement responses of the structural segment is higher than that of the damaged nearshore pile.

In brief, under the excitation of an abrupt unloading load, the displacement response distribution characteristics of all measurement points in the structural sediment of the high-piled wharf under 43 kinds of damage conditions have certain regularity, and this regularity is closely related to the direction, which indicates that the distribution of damage-related information in the displacement response signal is likely to be closely associated with the direction.

7.3.2. Model performance based on directional dynamic displacement training sets

To verify the directional sensitivity of the CNN model to the displacement response, 6 training groups were constructed by combining the displacement response in different directions to illustrate the performance difference of the proposed 1D CNN model. The training accuracy and validation accuracy of the above 6 models are shown in Fig. 18.

From this figure, several main results can be summarized as follows: (a) The classification accuracies of the model trained by

training group no. 6, including the training accuracy and validation accuracy, are slightly lower than those of the model based on the dataset in component form. This indicates that the vertical displacement responses of the structure have very limited impacts on the damage identification accuracy of the DL model. It is reasonable to believe that the dynamic response consistent with the main vibration mode of the structure carries more damage-sensitive information. The performance of the model trained by group no. 2 also led to the same conclusion. (b) The classification accuracies of model no. 4 and model no. 1 were significantly higher than those of model no. 5 and model no. 3, implying that the contribution of the longitudinal displacement response component to the classification accuracy of the SDIM was significantly superior to that of the lateral displacement response component of the structure. (c) The validation accuracy of the model no. 6 was significantly more discrete than that of the model based on the dataset in component form. Furthermore, the generalization abilities of model no. 4 and model no. 5 significantly outperform those of model no. 1 and model no. 3. These phenomena further confirm that the vertical displacement response components of the structural segment of the high-pile wharf have a pronounced effect on improving the generalization and robustness of the 1D CNN model.

8. Conclusions

This paper presented a novel structural damage detection framework for high-pile wharf foundations based on a uniting finite element method and deep learning. Based on the results obtained in this study, the following conclusions can be drawn:

1. This study was the first to apply a 1D CNN-based approach to the vibration-based structural damage detection of typical high-pile wharf foundations. The results indicated the superior performance of the 1D CNNs to learn the extraction of damage-sensitive features directly from the raw displacement response data. The proposed algorithm possesses excellent generalization and robustness by eliminating the need for any hand-crafted feature extraction in the parametric methods. Therefore, the established method has promising application prospects for the real-time SHM of port structures.

2. The novel SDD framework in this study has two components: the establishment of a reasonable FE model and the realization of efficient DL algorithms. The “m” method, which calculates the depth of the embedding point of the pile, is shown to be useful for simplified structural modeling for SHM purposes. Besides, the sample datasets required for the training of the proposed CNNs can be directly reconstructed by the displacement response time series of all the beam-pile nodes of the FE model, avoiding the complicated calculation process of the parameter identification method or the model correction method.

3. The computational complexity of the compact 1D CNNs is significantly lower because data processing involves only simple 1D operations (scalar multiplications and additions). Additionally, the damage condition labeling method based on one-hot coding can greatly improve the training efficiency of CNNs. Therefore, the proposed approach is computationally inexpensive in practice, which makes it suitable for SHM applications to other large civil structures.

4. The comprehensive performance of the CNNs based on the displacement response dataset in component form is significantly better than that based on the dataset in absolute value form. The latter training set greatly compresses the dimension of the displacement data. Although it is conducive to saving computational resources, it leads to the loss of more damage-related information, which is detrimental to the model learning process.

5. The proposed CNNs are more sensitive to the longitudinal and lateral displacement responses at the beam-pile nodes of the high-pile wharf structure. More specifically, the former has a higher contribution to the classification accuracy of CNNs than the latter; furthermore, their effects significantly outweigh the influence of vertical displacement. The displacement responses in the two plane directions above obviously contain more damage features of pile foundations, and it is reasonable to believe that there is more damage-sensitive information along with the main vibration mode directions of the structure. Although the contribution of the vertical displacement response to the improvement of the model identification accuracy is rather limited, this component has a positive effect on the improvement of the generalization and robustness of the CNNs.

6. The convolutional blocks consisted of linear connection of 2 1D convolutional layers and 1 max-pooling layer could effectively extract the damage-sensitive features with space and time translational invariance from the dynamic responses of the high-pile wharf, which significantly improve the efficiency of the SDD model based on 1D CNNs.

As the preliminary work of a field validation, the proposed method in this paper is highly exploratory, and its practical efficacy needs further investigations. The research team will conduct a field test under available conditions to verify the feasibility of the method.

CRediT authorship contribution statement

Yujue Zhou: Conceptualization, Methodology, Software, Formal analysis, Investigation, Writing – original draft, Writing – review & editing, Data curation. **Yonglai Zheng:** Resources, Project administration, Funding acquisition. **Yongcheng Liu:** Conceptualization, Methodology, Software, Formal analysis, Investigation, Writing – original draft, Writing – review & editing, Validation. **Tanbo Pan:** Formal analysis, Investigation, Writing – original draft, Data curation. **Yubao Zhou:** Formal analysis, Investigation, Writing – original draft.

Declaration of Competing Interest

The authors declare that they have no known competing financial interests or personal relationships that could have appeared to influence the work reported in this paper.

Acknowledgments

This study was supported by programs of Provincial Key Laboratory of Construction Materials & Structural Reinforcement, Sanming University, Sanming, China.

Appendix A

A.1. Forward propagation process

It is assumed that the CNNs have m layers with 1 layer input layer, 1 output layer, and m-2 layers for the hidden layer in the middle. The FP process is as follows:

$$\begin{aligned} Y^{(2)} &= W^{(1)}x + b^{(1)} \\ Z^{(2)} &= f(Y^{(2)}) \\ Y^{(3)} &= W^{(2)}Z^{(2)} + b^{(2)} \\ Z^{(3)} &= f(Y^{(3)}) \\ &\vdots \\ h_{W,b}(x) &= Z^{m} = f(Y^{m}) \end{aligned} \tag{1}$$

where x is the original input sample, $Y^{(i)}$ represents the input of the ith layer of the CNN, $W^{(i)}$ and $b^{(i)}$ are respectively the weight matrix and bias matrix of the ith layer, $Z^{(i)}$ is the output of the ith layer, $f(\bullet)$ is the activation function, and $h_{W,b}(x)$ is the final output of the CNNs.

A.2. Backpropagation process

In general, the training dataset contains a total of n samples, $\left[\left(x^{1}, y^{1}\right), \cdots, \left(x^{m}, y^{m}\right)\right]$. The loss function of the CNNs under the batch training strategy can be expressed as:

$$\begin{aligned} L(W,b) &= \left[\frac{1}{n}\sum_{i=1}^{n} L\left(W, b, x^{i}, y^{i}\right)\right] + \frac{\lambda}{2}\sum_{l=1}^{m_l-1}\sum_{i=1}^{m_i}\sum_{j=1}^{s_j+1} W_{ij}^{l} \\ &= \left[\frac{1}{m}\sum_{i=1}^{m}\frac{1}{2}\left\|h_{W,b}\left(x^{(i)}\right) - y^{i}\right\|\right] + \frac{\lambda}{2}\sum_{l=1}^{m_l-1}\sum_{i=1}^{m_i}\sum_{j=1}^{s_j+1} W_{ij}^{l} \end{aligned} \tag{2}$$

in the formula, the first term is the mean squared error between the single-batch network output and the error value of target output. The other term is the regularization term of the network weight, which is mainly used to suppress the degree of dispersion and absolute value of the weight matrix and prevent overfitting during the training process.

The update expressions of the network weight and bias value are:

$$\begin{aligned} W_{ij}^{l} &= W_{ij}^{l} - \alpha\frac{\partial}{\partial W_{ij}^{l}} L(W,b) \\ b_{i}^{(l)} &= b_{i}^{(l)} - \alpha\frac{\partial}{\partial b_{i}^{(l)}} L(W,b) \end{aligned} \tag{3}$$

where α represents the learning rate in the gradient descent algorithm, which is used to suppress the local optimal trap in the training process. The calculation formulas of the partial derivative terms of the network weight and bias value are as follows:

$$\begin{aligned} \frac{\partial}{\partial W_{ij}^{(l)}} L(W,b) &= \left[\frac{1}{n}\sum_{i=1}^{n}\frac{\partial}{\partial W_{ij}^{(l)}} L\left(W, b, x^{(i)}, y^{(i)}\right)\right] + \lambda W_{ij}^{(l)} \\ \frac{\partial}{\partial b_{i}^{(l)}} L(W,b) &= \frac{1}{n}\sum_{i=1}^{n}\frac{\partial}{\partial b_{i}^{(l)}} L\left(W, b, x^{(i)}, y^{(i)}\right) \end{aligned} \tag{4}$$

Appendix B

Fig. B1

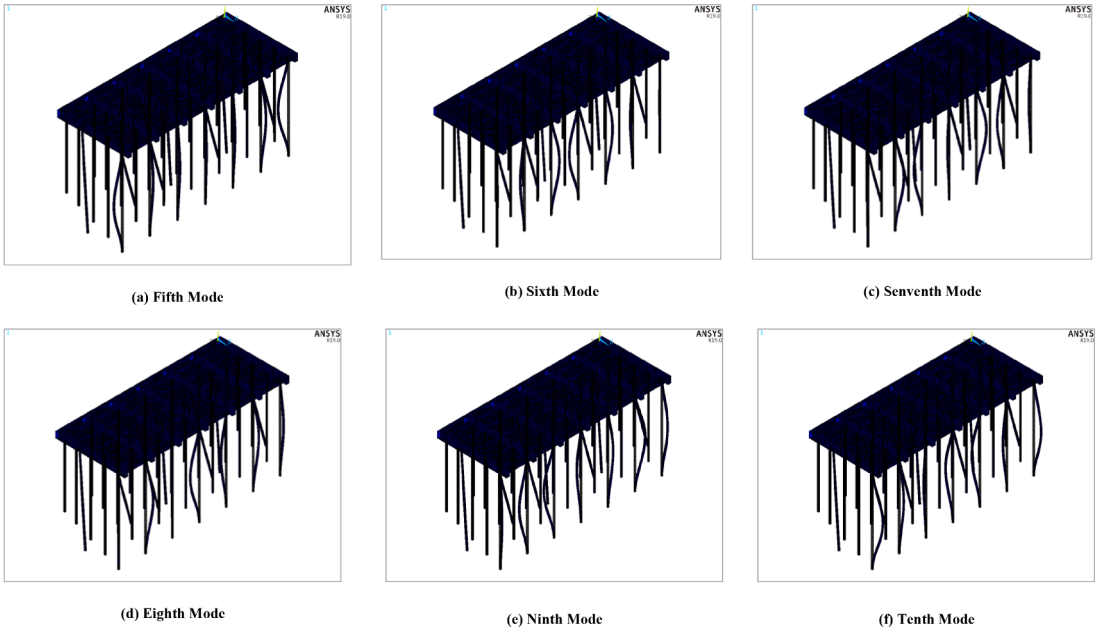

Fig. B1. The fifth to tenth modes of vibration of the typical high-pile wharf.

References

[1] Y. Zheng, Y. Zhou, Y. Zhou, T. Pan, L. Sun, D. Liu, Localized corrosion induced damage monitoring of large-scale RC piles using acoustic emission technique in the marine environment, Constr. Build. Mater. 243 (2020), 118270.
[2] J. Long, O. Buyukozturk, Automated structural damage detection using one-class machine learning, Dynamics of Civil Structures, Volume 4, Springer, 2014, pp. 117-128.
[3] O. Avci, O. Abdeljaber, S. Kiranyaz, M. Hussein, M. Gabbouj, D.J. Inman, A Review of Vibration-Based Damage Detection in Civil Structures: From Traditional Methods to Machine Learning and Deep Learning Applications, arXiv preprint arXiv:2004.04373, (2020).
[4] R. Ghiasi, P. Torkzadeh, M. Noori, A machine-learning approach for structural damage detection using least square support vector machine based on a new combinational kernel function, Struct. Health Monit. 15 (2016) 302–316.
[5] W. Fan, P. Qiao, Vibration-based damage identification methods: a review and comparative study, Struct. Health Monitor. 10 (2011) 83–111.
[6] R. Hou, Y. Xia, Review on the new development of vibration-based damage identification for civil engineering structures: 2010–2019, J. Sound Vib. 115741 (2020).
[7] C.R. Farrar, S.W. Doebling, D.A. Nix, Vibration–based structural damage identification, Philos. Trans. R. Soc. London Series A 359 (2001) 131–149.
[8] H.W. Shih, D.P. Thambiratnam, T.H. Chan, Vibration based structural damage detection in flexural members using multi-criteria approach, J. Sound Vib. 323 (2009) 645–661.
[9] O. Abdeljaber, O. Avci, Nonparametric structural damage detection algorithm for ambient vibration response: Utilizing artificial neural networks and self-organizing maps, J. Archit. Eng. 22 (2016) 04016004.
[10] S.W. Doebling, C.R. Farrar, M.B. Prime, A summary review of vibration-based damage identification methods, Shock and Vibration Digest 30 (1998) 91–105.
[11] F. Magalhães, Á. Cunha, E. Caetano, Vibration based structural health monitoring of an arch bridge: from automated OMA to damage detection, Mech. Syst. Sig. Process. 28 (2012) 212–228.
[12] O. Avci, O. Abdeljaber, S. Kiranyaz, D. Inman, Structural damage detection in real time: implementation of 1D convolutional neural networks for SHM applications, in: Structural Health Monitoring & Damage Detection, Springer, 2017, pp. 49–54.
[13] E. Figueiredo, A. Santos, Machine learning algorithms for damage detection, Vibration-Based Techniques for Damage Detection and Localization in Engineering Structures, (2018) 1-39.
[14] E. Figueiredo, G. Park, C.R. Farrar, K. Worden, J. Figueiras, Machine learning algorithms for damage detection under operational and environmental variability, Struct. Health Monit. 10 (2011) 559–572.
[15] S. Sharma, S. Sen, One-dimensional convolutional neural network-based damage detection in structural joints, J. Civil Struct. Health Monitor. 10 (2020) 1057–1072.
[16] Y. Sarawgi, S. Somani, A. Chhabra, Nonparametric vibration based damage detection technique for structural health monitoring using 1D CNN, in: International Conference on Computer Vision and Image Processing, Springer, 2019, pp. 146–157.
[17] O. Abdeljaber, O. Avci, S. Kiranyaz, M. Gabbouj, D.J. Inman, Real-time vibration-based structural damage detection using one-dimensional convolutional neural networks, J. Sound Vib. 388 (2017) 154–170.
[18] O. Avci, O. Abdeljaber, S. Kiranyaz, M. Hussein, D.J. Inman, Wireless and real-time structural damage detection: a novel decentralized method for wireless sensor networks, J. Sound Vib. 424 (2018) 158–172.
[19] O. Avci, O. Abdeljaber, S. Kiranyaz, D. Inman, Convolutional Neural Networks for Real-time and Wireless Damage Detection, Dynamics of Civil Structures, Volume 2, in: Proceedings of the 37th IMAC, A Conference and Exposition on Structural Dynamics 2019, 2019, p. 129.
[20] O. Avci, O. Abdeljaber, S. Kiranyaz, B. Boashash, H. Sodano, D.J. Inman, Efficiency validation of one dimensional convolutional neural networks for structural damage detection using a SHM benchmark data, Proc. 25th Int. Conf. Sound Vib.(ICSV), 2018, pp. 4600-4607.

[21] O. Abdeljaber, O. Avci, M.S. Kiranyaz, B. Boashash, H. Sodano, D.J. Inman, 1-D CNNs for structural damage detection: verification on a structural health monitoring benchmark data, Neurocomputing 275 (2018) 1308–1317.
[22] Code for Pile Foundation of Harbor Engineering, in: I. Standard-Transportation (Ed.) JTS 167-4-2012, China, ,2012 (in Chinese).
[23] G.F. Gomes, F.A. de Almeida, S.S. da Cunha, A.C. Ancelotti, An estimate of the location of multiple delaminations on aeronautical CFRP plates using modal data inverse problem, Int. J. Adv. Manuf. Technol. 99 (2018) 1155–1174.
[24] M. Jin, Damage identification methods based on structural response vectors and machine learning algorithms, College of Civil Engineering and Transportation, South China University of Technology, 2019. (in Chinese).
[25] R.L. Boroschek, H. Baesler, C. Vega, Experimental evaluation of the dynamic properties of a wharf structure, Eng. Struct. 33 (2011) 344–356.
[26] L. Cheng, Q. Wang, H. Peng, The vibration measurement and analysis of piled wharf, J. Disaster-Prevent. Sci. Technol. 13 (2011) 42–46, in Chinese.
[27] P.J. Roache, Quantification of uncertainty in computational fluid dynamics, Annu. Rev. Fluid Mech. 29 (1997) 123–160.
[28] A. Khan, A. Sohail, U. Zahoora, A.S. Qureshi, A survey of the recent architectures of deep convolutional neural networks, Artif. Intell. Rev. 53 (2020) 5455–5516.
[29] S.W.F. de Rezende, J.d.R.V. de Moura, R.M.F. Neto, C.A. Gallo, V. Steffen, Convolutional neural network and impedance-based SHM applied to damage detection, Eng. Res. Express 2 (2020), 035031.
[30] S. Kiranyaz, T. Ince, M. Gabbouj, Real-time patient-specific ECG classification by 1-D convolutional neural networks, IEEE Trans. Biomed. Eng. 63 (2015) 664–675.